Tensile Properties and Structure of Several Superalloys after Long-Term Exposure to LiF and Vacuum at 1173 K

J.D. Whittenberger

The use of the solid-to-liquid phase transformation of LiF to store thermal energy is under consideration for a space-based solar dynamic system. Although advantageous in terms of its energy density, the melting point of this salt (1121 K) is beyond the commonly accepted upper-use temperature of 1100 K for chromium-bearing superalloys in vacuum. However, one commercially available nickel-base superalloy (Hastelloy B-2) is chromium free; unfortunately, because of its high molybdenum content, this alloy can form phases that cause high-temperature embrittlement. To test the suitability of Hastelloy B-2, it has been exposed to molten LiF, its vapor and vacuum at 1173 K for 2500, 5000, and 10^4 h. For control, the chromium-containing cobalt-base Haynes alloy 188 and nickel-base Haynes alloy 230 were also exposed to LiF and vacuum at 1173 K for 5000 h. Neither LiF nor vacuum exposures had any significant effect on Hastelloy B-2 in terms of microstructural surface damage or weight change. Measurement of the post exposure tensile properties of Hastelloy B-2, nevertheless, revealed low tensile ductility at 1050 K. Such embrittlement and low strength at elevated temperatures appear to preclude the use of Hastelloy B-2 as a containment material for LiF. Little evidence of significant attack by LiF was seen in either of the chromium-containing superalloys; however, considerable weight loss and near-surface microstructural damage occurred in both alloys exposed to vacuum. Although measurement of the post exposure room-temperature tensile properties of Haynes alloys 188 and 230 revealed no significant loss of strength or ductility, the severe degree of microstructural damage found in unshielded alloys exposed to vacuum indicates that chromium-bearing superalloys might also be unsuitable for prolonged containment of LiF in space above 1100 K.

Keywords

chemical compatibility, Hastelloy B-2, Haynes alloy 188, Haynes alloy 230, microstructure, superalloys, tensile properties, thermal energy storage

Editor's Note:

This is the final paper on a NASA-sponsored activity on containment of thermal energy storage materials (LiF, LiF-CaF_2, LiOH) for space power applications.

All the work has been documented over the last eight years in ASM International's *Journal of Materials Engineering and Performance* and its predecessor ASM journals:

J. Mater. Eng., Vol 8, 1987, p 385-390
J. Mater. Eng., Vol 9, 1987, p 293-302
J. Mater. Eng., Vol 10, 1988, p 247-258
J. Mater. Eng., Vol 12, 1990, p 211-226
J. Mater. Eng., Vol 13, 1991, p 257-271
J. Mater. Eng. Perform., Vol 1, 1992, p 469-482
J. Mater. Eng. Perform., Vol 2, 1993, p 745-757
J. Mater. Eng. Perform., Vol 3, 1994, p 91-103
J. Mater. Eng. Perform., Vol 3, 1994, p 754-762
J. Mater. Eng. Perform., Vol 3, 1994, p 763-774

ASM considers it a privilege to contribute to the dissemination of this important data and information as part of the worldwide effort in space exploration.

J.D. Whittenberger, NASA Lewis Research Center, Cleveland, OH, USA.

1. Introduction

LONG-TERM manning of earth-orbiting space stations requires efficient, dependable sources of electrical power. Although the initial energy supply for the Space Station will utilize photovoltaic arrays, solar dynamic systems offer greater efficiency in a more compact form (Ref 1). A solar dynamic system typically possesses five major components: (1) a focused mirror to gather sunlight, (2) a receiver to absorb the energy, (3) a thermal energy storage system to retain the heat, (4) a heat engine (i.e., a Rankine/Brayton turbine or Stirling engine), and (5) an electrical generator. Each component has difficulties with materials; however, those associated with the energy storage could be particularly troublesome, because the latent heat of a solid-to-liquid phase transformation appears to be the most efficient mechanism to store large quantities of energy at high temperatures. Of the available candidate materials for energy storage, fluoride-based salts are the most advantageous in terms of both energy per mass and energy per volume (Ref 2, 3).

Proposals for the first generation of space-based solar dynamic systems have involved a low-temperature (~1015 K) Brayton Cycle heat engine (Ref 4) in combination with the eutectic salt LiF-20CaF_2,* which melts at 1043 K. Such a relatively low operating temperature was chosen to allow the use of conventional wrought superalloys for the high-temperature hardware (Ref 5-8) and because of reluctance to build the initial system from refractory alloys. To ensure that salt corrosion presented no unexpected problems, long-term exposures (Ref 9-12) of several conventional superalloys—the cobalt-base Haynes alloy 188 and the nickel-base Haynes alloy 230 (Haynes International, Kokomo, IN) and Inconel 617 (International Nickel Company, Huntington, WV)—have been under-

*All compositions of thermal energy storage salts are in mole percent.

Table 1 Characterization of starting materials

Material	Vendor	Heat/lot	Composition, wt%
Hastelloy B-2	Cabot Corp.	266556265	<0.002C, <0.1Co, 0.24Cr, 0.74Fe, 0.12Mn, 27.7Mo, <0.005P, <0.002S, <0.02Si, bal Ni
Haynes alloy 188	Cabot Corp.	188061773	0.005B, 0.11C, 21.69Cr, 1.95Fe, 0.048La, 0.72Mn, 23.03Ni, 0.013P, <0.002S, 0.38Si, 14.02W, bal Co
Haynes alloy 230	Cabot Corp.	1830557171	0.004B, 0.3Al, 0.10C, 22.00Cr, 1.22Fe, 0.009La, 0.61Mn, 1.29Mo, 0.01P, <0.002S, 0.39Si, 14.01W, bal Ni
Ni 201	DVN America	6510	0.02C, 0.01Cu, 0.06Fe, 0.001S, 0.16Si, bal Ni
LiF(a)	Cerac, Inc.	27230-A-11	0.001Al, 0.01Ca, 0.001Cu, 0.005Fe, 0.01Mg, 26.78Li, bal F

(a) Chemical analysis of the as-received LiF by inductively coupled plasma emission spectrometry at the Lewis Research Center indicated: B, Ba, Co, Cr, Mn, Mo, Na, Nb, Ni, Pb, Si, Sn, Ti, V, W, Y, Zr < 1ppm.

taken in the near-eutectic salt LiF-22CaF_2 at 1093 K. These experiments demonstrated that neither the molten eutectic salt nor its vapor produce any changes in the structure or simple mechanical properties beyond those attributable to simple thermal exposure. Furthermore, compared to long-term air exposures at 1093 K (Ref 13, 14), the effects of similar-length heat treatments in LiF-22CaF_2 environments were no worse and perhaps not as severe.

Although the latent heat of fusion for the eutectic LiF-20CaF_2 has high energy densities (0.82 MJ/kg and 1.7 GJ/m^3 [Ref 2]), the use of pure LiF can provide significant improvement (1.08 MJ/kg and 1.96 GJ/m^3 [Ref 2]). Therefore, for the same energy storage capacity, the weight of LiF would be about 30% lower than that required for LiF-20CaF_2, and the volume of LiF would be about 15% less than the eutectic. This decrease in volume could also result in a further weight savings by reducing the amount of material required to contain the thermal energy storage salt. While advantageous, the replacement of LiF-20CaF_2 by LiF would also entail an approximately 80 K higher operating temperature due to the 1121 K melting point for pure LiF. This could create additional material demands on all high-temperature components. In terms of the LiF containment vessels, previous studies of stainless steels and superalloys in contact with molten LiF (Ref 5-8) have shown that this salt has little adverse effect on metals with low aluminum + titanium content (<4 wt%) as long as "pure" LiF is utilized. In particular, caution must be exerted to ensure that entrained water in the salt is removed before the thermal energy storage vessels are filled with the LiF. As little as 100 ppm H_2O can lead to chemical reactions that corrode the containment alloy and produce internal gas pressures on the order of 0.25 atm (Ref 2).

With the increased melting point of LiF in comparison to the LiF-20CaF_2 eutectic, long-term exposure to the vacuum of space must now be considered as a hostile environment. In general, the stability of metals alloyed with volatile elements (chromium, manganese, etc.) is of concern at temperatures exceeding approximately 1100 K. This was demonstrated more than 25 years ago by Bourgette (Ref 15-18), who heat treated a number of wrought stainless steels and superalloys in vacuum and found examples of selective evaporation. Although vacuum levels between approximately 10^{-3} and 10^{-7} Pa had little influence on the loss of chromium and manganese, volatilization rates increased with temperature and decreased with accumulating time of exposure. Such behavior was consistent with diffusional processes bringing the volatile species to the metal surface. In such near-surface diffusion zones, visible changes in the microstructure were seen. These included Kirkendall porosity and grain-boundary voids, dissolution of some precipitates (i.e., chromium carbides), enhancement of other precipitates (i.e., Laves phases in cobalt-base alloys), and phase transformations (austenite to ferrite in stainless steels). While no direct evidence was noted (Ref 16) that these changes affected mechanical behavior, it was hypothesized that they would ultimately do so.

If 1100 K is the boundary between acceptable and unacceptable application of Cr(Mn)-containing superalloys in vacuum, then perhaps a non-chromium-containing superalloy would be successful. In reality, only one commercially available, essentially chromium-free wrought superalloy could be found: Hastelloy B-2 (Haynes International, Kokomo, IN). Although this material contains very low amounts of volatile or LiF-reactive elements, its high molybdenum content leads to embrittlement at elevated temperatures when heated between 810 and 1090 K through the formation of Ni_3Mo and Ni_4Mo (Ref 19). This could pose a problem even though the melting point of LiF is about 30 K above the upper limit for embrittlement. Certainly during start-up or shutdown cycles, containment alloy temperatures will pass through the embrittlement regime; furthermore, during actual operation as energy is being withdrawn from the molten salt, it is possible that the metal temperatures will decrease below 1090 K.

To determine the viability of Hastelloy B-2 as a containment alloy for LiF in a space-based environment, large numbers of tensile-type samples have been exposed for periods up to 10^4 h to these environments at 1173 K in "bread pan" capsules. Because previous studies of 1093 K vacuum-exposed chromium-containing superalloys (Ref 13) demonstrated no significant volatilization, intermediate-term exposures (~5000 h) of the cobalt-base superalloy Haynes alloy 188 and the nickel-base Haynes alloy 230 to LiF and vacuum were also undertaken. This paper reports the results of the salt/vacuum exposures on the behavior, structure, and simple tensile properties of these three alloys.

2. Experimental Procedures

2.1 *Hastelloy B-2*

Several 1.6 mm thick by 0.6 m by 1.2 m sheets of Hastelloy B-2 (Table 1) were purchased for this study. This material was supplied in a solution-treated condition (1340 K, rapidly quenched) and possessed a normal silver metallic sheen. Metallographic examination of polished, unetched sections re-

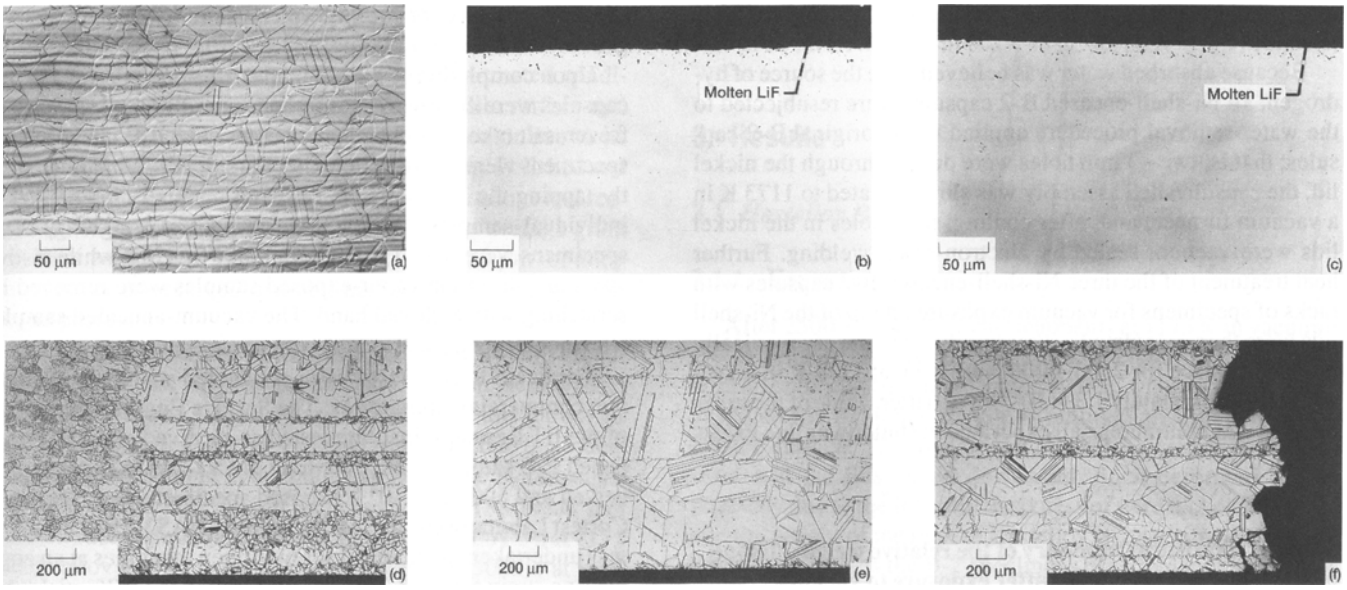

Fig. 1 Typical microstructures of as-received and exposed Hastelloy B-2. (a) As received. (b) Near-surface porosity after 10^4 h exposure to molten LiF at 1173 K. (c) Specimen rack after 2500 h exposure to molten LiF at 1173 K. (d) GTA weld/sheet junction after 2500 h at 1173 K. (e) Sheet after 10^4 h at 1173 K. (f) Fracture in specimen rack after 10^4 h exposure to molten LiF at 1173 K. (a, d-f) Etched. (b, c) Unetched

vealed that as-received alloy B-2 sheet had a uniform cross section with no visible second phases or porosity in the unetched state. After etching, an equiaxed grain structure (~34 μm in diameter with a 3 μm standard deviation) with many twins and residual traces from deformation bands was found (Fig. 1a).

Following the procedures outlined in Ref 9 to 12, three bread-pan-shaped capsules, about 280 mm long by 140 mm high and 115 mm wide, with matching lids and specimen racks and designed to hold about 50 tensile test specimens each, were fabricated from the sheet material. Pin-and-clevis tensile-type test samples, 101.6 mm long, by 19 mm wide with a 31.8 mm by 9.5 mm gage section, were punched from the alloy sheet with the gage length parallel to the sheet rolling direction. After the tensile specimens were cleaned by hot vapor degreasing in trichloroethane followed by immersion within an ultrasonic bath, they were individually weighed and measured. Samples were then placed into specimen racks and recleaned along with bread pans and lids.

With a rack of specimens on the bottom of the capsule, about 2.6 kg of LiF chunks (Table 1) were poured into the bread pan. After the second rack was placed on tabs within the capsule, the lid (which contained two ~3 mm holes) was gas tungsten arc (GTA) welded in an argon atmosphere to the main body. This assembly was then heat treated at 1173 K in a diffusion-pumped vacuum furnace (8 h from room temperature to 1073 K, 2 h to 1173 K, followed by 1 h hold at temperature and a furnace cool under vacuum) to remove dissolved gases and water from the salt. While somewhat warm (~325 K), the vacuum furnace was backfilled with air; the assembly was removed, immediately transported to an electron-beam welding facility, and placed under vacuum. The holes in the lids were then closed by electron-beam welding.

Each B-2 capsule, with its accompanying third rack of specimens for the vacuum exposure placed on the lid, was individually vacuum heat treated by heating for 24 h at 1173 K in the diffusion-pumped vacuum furnace and examined for salt leaks after cooling. Although no direct evidence for large or even small leaks was seen, several darkish areas near the electron-beam welds on one capsule were observed. All three capsules were then placed in a large cryogenically pumped vacuum furnace for prolonged heat treatment; however, after about 125 h the furnace turned itself off due to a loss of pumping capacity. When the vacuum chamber was opened, salt deposits were found on the cold portions of the thermal heat shields, and cracks were detected in the heat-affected zones surrounding all the electron-beam welds. Since no other B-2 capsules were available for use, the cracked bread pans were vacuum sealed inside larger Ni-201 (Table 1) shells of similar geometry (approximately 300 mm long by 160 mm high and 130 mm wide with matching lids) following the procedure outlined in Ref 12. Prior to placing the Hastelloy B-2 capsules in their Ni-shells, several holes were drilled into each capsule to ensure that air was removed during vacuum sealing.

Initial attempts to heat treat the first Ni-shell-encased B-2 capsule (with its accompanying third rack of specimens for the vacuum exposure placed on the shell lid) in the cryogenic vacuum furnace were not successful, as hydrogen was evolved during heat-up and poisoned the cryopump. The most logical source for this hydrogen was water absorbed by the LiF during handling of the cracked capsules in air. During heating, this water would then react with the salt to form gaseous H_2O and HF (Ref 2). These, in turn, established a partial pressure of hydrogen gas in the Ni-shell, which then permeated through the walls. Hydrogen permeation had been previously identified as the cause for shutdowns of cryogenic vacuum pumps during at-

tempts to heat treat pure Ni/LiOH corrosion capsules at 775 K (Ref 20).

Because absorbed water was believed to be the source of hydrogen, all Ni-shell-encased B-2 capsules were resubjected to the water-removal procedure applied to the original B-2 capsules; that is, two ~3 mm holes were drilled through the nickel lid, the capsule/shell assembly was slowly heated to 1173 K in a vacuum furnace, and, after cooling, both holes in the nickel lids were vacuum sealed by electron-beam welding. Further heat treatment of the three Ni-shell-encased B-2 capsules with racks of specimens for vacuum exposure on top of the Ni-shell lids were then completed without problem in the cryogenically pumped furnace for 2500, 5000, and 10^4 h at 1173 K in a vacuum of approximately 1.3×10^{-4} Pa or better. None of these exposures was continuous; all experienced shutdowns due to loss of electrical power or cooling water, vacuum furnace leaks, regeneration of the cryopumps, and so forth.

Table 2 Statistical summary of the relative weight change of Hastelloy B-2 specimens after exposure to various environments at 1173 K

	(Exposed – as-received)(a), mg/cm^2		
Length of exposure, h	Molten salt	Salt vapor	Vacuum
2500			
Average	0.13	0.16	0.58
Std. dev.	0.02	0.20	0.08
Maximum	0.16	0.77	0.89
Minimum	0.08	–0.07	0.42
5000			
Average	0.12	0.20	0.70(b)
Std. dev.	0.02	0.07	0.04
Maximum	0.17	0.30	0.79
Minimum	0.07	0.03	0.62
10,000			
Average	0.12	–0.05	0.99
Std. dev.	0.04	0.02	0.11
Maximum	0.29	–0.003	1.75
Minimum	0.08	–0.09	0.83

(a) Data from about 50 specimens for each condition, where each sample has about 33 cm^2 of surface area and weighs about 22 g. (b) Data from the two end specimens were not included; these had one side completely covered with the dark scale. Weight gain for both of these specimens was about 33 mg.

Upon completion of the planned corrosion experiments, the capsules were cut open, photographed, and several samples of frozen salt taken for chemical analysis. The LiF-encapsulated specimens were freed by breaking the salt with a hammer, gently tapping the shoulder sections, and manually manipulating individual samples. Prior to measuring and weighing, these specimens were wiped with a clean, lint-free rag, while visible spots of salt on the vapor-exposed samples were removed by scratching with a gloved hand. The vacuum-annealed samples were not cleaned prior to postexposure measurements.

Triplicate tensile tests were conducted under contract by two commercial laboratories: The Surface Engineering Center of the IIT Research Institute tested as-received and 2500 h exposed B-2 samples under contract NAS3-24976, while as-received and 5000 and 10^4 h exposed specimens were tested by Cortest Laboratories, Inc. under contract NAS3-25759. Testing was undertaken in universal screw-driven machines at an engineering strain rate of 8.3×10^{-5} s^{-1} through the 0.2% yield; beyond this strain, the engineering strain rate was increased to 8.3×10^{-4} s^{-1} and held until failure. Strain was measured via a mechanical extensometer directly attached to the gage section. The testing atmosphere varied with temperature: (1) At 77 K, specimens were immersed in liquid N_2; (2) at 298 K, tests were conducted in air; and (3) at and above 750 K, measurements were carried out in a 0.006 Pa or better vacuum. Typical test data included 0.02 and 0.2% offset yield strengths, ultimate tensile strength (UTS), and elongation at failure; all mechanical properties were calculated on the basis of the original (preexposure) dimensions.

Standard metallographic procedures and chemical analysis were employed for characterization. When required, the B-2 was electrolytically etched at 4 V and 0.5 A in 95 ml H_2O plus 5 ml HCl or 95 ml H_2O plus 5 ml HF.

2.2 *Haynes Alloys 188 and 230*

Single bread-pan capsules and associated racks of specimens were also fabricated from alloy 188 and alloy 230 (Table 1) sheet following the same procedure outlined above. Both of these materials were supplied by Haynes International in the form of approximately 1.27 mm thick by 0.6 m by 1.2 m sheets.

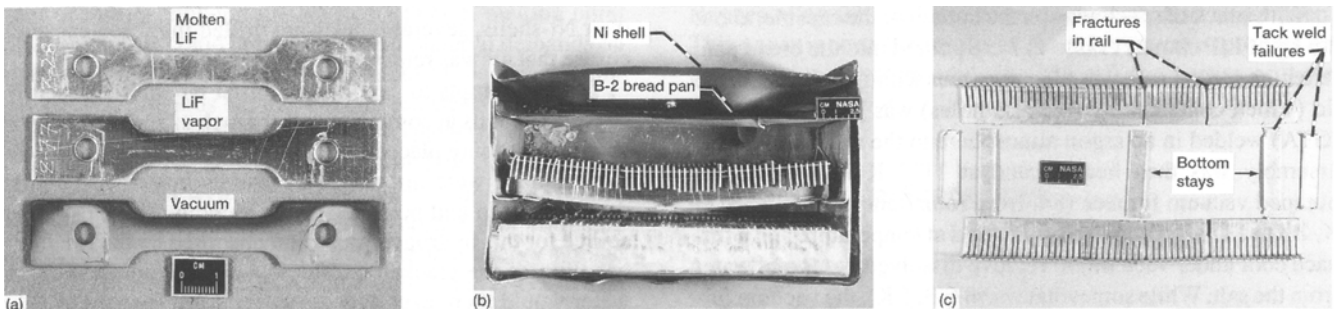

Fig. 2 (a) LiF- and vacuum-exposed Hastelloy B-2 tensile samples after 5000 h at 1173 K. (b) An opened B-2 bread-pan capsule encased by a Ni-shell after 10^4 h at temperature. (c) Fractured B-2 specimen rack that held the tensile samples in molten LiF after 10^4 h at temperature

Characteristics of the as-received alloys have been well documented (Ref 9-14) and will not be repeated here in detail. In brief, the materials were supplied in a solution-treated condition, with alloy 188 sheet having a silver metallic surface and alloy 230 sheet having a dull oxide-like gray color due to its black anneal + pickling surface finish processing. Polished and etched metallurgical sections revealed that both alloys had reasonably uniform, equiaxed grain structures; the average grain diameters were about 35 μm for alloy 230 and 20 μm for alloy 188. Neither as-received material had significant amounts of second phases.

During heat treatment of the alloy 188 and alloy 230 bread-pan capsules, a salt leak was found near a weld on the alloy 188 capsule after about 100 h of exposure. Hence, this particular capsule was encased in a Ni-shell and resubjected to the water-removal heat treatment in the same manner as the B-2 capsules described above. The Ni-shell-encased alloy 188 bread pan was then successfully heat treated for a total of 5001.3 h at 1173 K. The alloy 230 capsule was heat treated for 5000 h at temperature without being encased in a Ni-shell; however, examination of this capsule after completion of the heat treatment revealed a small salt leak in a weld. As the capsule was examined after 2608 h of exposure and no evidence for any weld failures was observed, the leak developed during the last 2400 h of heat treatment.

Examination of the alloy 188 and alloy 230 capsules after their planned exposures was the same as that for B-2 capsules; however, because of a funding limitation, only room-temperature tensile properties were measured on as-received and exposed (molten LiF, its vapor, and vacuum) alloys. Such tests were conducted on a screw-driven machine initially operating at an engineering strain rate of 8.3×10^{-5} s^{-1} for the first few percent of deformation, after which the engineering strain rate was increased to 8.3×10^{-4} s^{-1} and held constant until fracture. A clip-on 12.4 mm gage length extensometer was attached to the center of the specimen gage section and use to monitor the first approximately 8% strain.

Standard metallographic procedures were used to characterize exposed and room-temperature-tested materials. Alloy 188 was electrolytically etched at 2 V in 95 ml H_2O plus 5 ml HCl, while alloy 230 was electrolytically etched at 2 V in a mixture of 33 ml HNO_3, 33 ml H_2O, 33 ml acetic acid, and 1 ml HF.

3. Results

3.1 *Hastelloy B-2*

3.1.1 Exposures

After 2500 and 5000 h heat treatments at 1173 K in vacuum, the exterior of the Ni-201 shells was metallic in appearance with an outline of the nickel grains visible, whereas the Ni-shell annealed for 10^4 h had its grains outlined on a medium gray, frosted surface. The tops of the Ni-shells were all bowed inward and the lids caved downward. Such deformation was probably due to the inherent weakness of pure nickel at 1173 K and the weight of the rack of Hastelloy B-2 specimens lying on the lid. In all cases the B-2 specimens placed in racks on top of the Ni-shells for vacuum exposure were partially covered with darkish scale on the regions facing away from the Ni-shell, while the remaining portion of each specimen had a gray tarnish finish (Fig. 2a). X-ray analysis of the scales indicated that they were composed of a nickel-base spinel and Cr_2O_3. Such contamination was probably from the simultaneous exposure of alloys 188 and 230 along with B-2 in combination with air leaking into the vacuum furnace. In this case, volatile chromium would be vapor-transported from the two chromium-rich superalloys (sources) and deposited on the chromium-deficient B-2 (sink), where it could subsequently oxidize.

The interior of each bread pan was revealed by saw-cutting away the side walls of both the Ni-shell and the B-2 capsule; a typical example of an opened capsule is shown in Fig. 2(b). Frozen LiF was found at the bottom between the Ni-shell and the B-2 walls. The thickness of the salt in this region was approximately the same as the block of salt inside the bread pan. The clearly visible rack of specimens in Fig. 2(b) was exposed to the LiF vapor, and in all cases such racks were found to be bent downward, even after 2500 h of heat treatment. Visual examination of the LiF-vapor-exposed specimens revealed that they were bright and shiny metallic with some samples spotted

Table 3 Tensile properties of as-received Hastelloy B-2 as determined by several testing laboratories

Test	0.02 % Yield stress, MPa		0.2 % Yield stress, MPa		UTS, MPa		Elongation, %	
temperature, K	Average	Std. dev.	Average	Std. dev.	Average	Std. dev.	Average	Std. dev.
IIT Research Institute								
77	509.0	26.9	583.7	9.7	1222.7	18.9	57.3	14.0
298	407.7	1.2	442.7	2.6	899.7	13.9	52.7	3.1
750	305.3	18.4	342.7	8.4	780.0	8.8	41.7	0.5
900	334.7	20.2	353.7	18.0	513.3	9.0	13.3	1.7
1050								
1200								
Cortest Laboratories								
77	519.5	29.4	549.7	28.8	1270.7	7.5	56.6	1.5
298	388.1	29.4	423.7	14.8	939.6	5.1	52.1	2.1
750	317.9	1.7	340.0	1.7	800.1	10.6	45.0	1.2
900	327.5	17.0	348.6	12.5	582.2	15.8	16.9	1.5
1050	499.8	24.1	515.2	22.4	563.3	17.5	2.1	0.4
1200	256.5	9.6	269.9	3.9	279.4	5.4	13.3	3.1

Table 4 Tensile properties of Hastelloy B-2 after 2500 h exposure at 1173 K as measured by IIT Research Institute

Test	0.02% Yield stress, MPa		0.2% Yield stress, MPa		UTS, MPa		Elongation, %	
temperature, K	Average	Std. dev.	Average	Std. dev.	Average	Std. dev.	Average	Std. dev.
Molten LiF								
77	708.7	9.5	732.0	5.4	997.0	9.4	15.7	1.2
298	587.7	16.1	633.3	9.0	965.3	1.9	31.7	1.7
750	446.5	36.5	507.5	15.5	727.7	32.4	16.0	1.4
900	475.0	...	522.0	...	501.0	27.4	2.0	1.4
1050								
1200	117.3	28.4	126.0	29.7	208.7	9.1	13.0	2.2
LiF vapor								
77	626.3	15.0	691.3	2.5	1253.3	35.6	40.7	5.4
298	501.7	48.6	585.7	7.8	1008.7	4.9	47.7	4.0
750	466.7	21.6	488.0	12.0	824.7	1.2	38.0	2.9
900	485.5	10.5	494.0	14.0	524.0	13.0	1.5	0.5
1050								
1200	144.0	...	150.0	...	231.0	7.0	10.0	1.0
Vacuum								
77	445.3	30.4	519.7	4.0	1118.7	8.5	77.7	1.2
298	354.3	33.3	440.7	46.6	861.3	18.1	66.3	0.9
750	296.7	6.2	307.0	2.2	711.0	3.3	61.0	5.1
900								
1050								
1200								

Table 5 Tensile properties of Hastelloy B-2 after 5000 h exposure at 1173 K as measured by Cortest Laboratories

Test	0.02% Yield stress, MPa		0.2% Yield stress, MPa		UTS, MPa		Elongation, %	
temperature, K	Average	Std. dev.	Average	Std. dev.	Average	Std. dev.	Average	Std. dev.
Molten LiF								
77	538.9	6.2	544.8	4.0	1152.8	16.7	57.9	2.3
298	399.9	10.1	440.1	16.8	912.2	17.7	52.8	1.6
750	297.5	13.5	322.5	2.4	740.8	1.9	49.9	0.2
900	301.3	5.1	311.1	3.8	536.6	21.7	18.9	2.1
1050	410.6	11.8	434.4	9.9	442.1	14.5	1.6	0.3
1200	205.0	10.9	228.0	7.2	254.6	1.4	14.1	0.4
LiF vapor								
77	510.4	9.5	519.7	4.5	1133.6	38.5	58.3	8.1
298	399.8	3.3	407.5	10.3	890.3	6.6	56.1	1.3
750	287.5	9.7	311.9	8.8	742.6	3.3	52.0	0.6
900	287.7	14.8	301.0	11.6	623.5	13.6	30.9	3.5
1050	412.2	30.7	436.6	25.3	463.5	15.2	2.0	0.2
1200	201.3	14.3	209.8	13.0	265.2	4.3	14.6	0.2
Vacuum								
77	479.3	4.6	489.9	8.1	1085.6	13.5	65.4	4.2
298	348.7	6.6	356.9	3.2	838.2	9.0	62.7	1.0
750	252.8	5.9	269.5	9.2	693.6	7.3	52.0	0.6
900	244.0	6.1	247.7	4.1	564.7	7.2	29.9	0.7
1050	380.8	43.2	404.1	33.7	428.3	11.7	1.8	0.6
1200	185.2	8.0	201.6	3.6	251.0	2.5	12.9	1.1

with frozen salt (Fig. 2a). No signs of corrosion were found within or on the outside of the B-2 capsule except where the original weld failures occurred.

Immediately below the vapor-exposed samples was the translucent block of frozen salt (Fig. 2b) encasing the rack of specimens that was immersed in the molten LiF at temperature. Since the LiF did not adhere to the B-2, the samples were easily freed. The molten-salt-exposed samples were found to be bright metallic with patches of mottled gray. Surprisingly, the racks supporting the specimens in the molten LiF were broken into pieces after 5000 and 10^4 h heat treatments (Fig. 2c). Failures occurred both at tack weld joints between the stays and rails of the rack as well as in the rails themselves. Similar failures also occurred in the rack from the 2500 h capsule; however, in this case the final fracturing into pieces occurred during freeing of the salt-encased samples. The frozen LiF around and between the specimens was transparent; chemical analyses of the various samples of LiF from different locations in the capsules revealed no third elements beyond those found in the virgin LiF (Table 1).

Table 6 Tensile properties of Hastelloy B-2 after 10,000 h exposure at 1173 K as measured by Cortest Laboratories

Test	0.02 % Yield stress, MPa		0.2 % Yield stress, MPa		UTS, MPa		Elongation, %	
temperature, K	Average	Std. dev.	Average	Std. dev.	Average	Std. dev.	Average	Std. dev.
Molten LiF								
77	675.9	15.0	706.4	15.2	982.9	9.5	14.7	1.0
298	548.3	14.8	618.1	20.8	894.6	20.3	25.1	2.6
750	489.7	15.4	498.6	18.7	534.6	8.9	20.1	1.3
900	261.2	9.9	274.9	13.8	618.4	15.5	16.4	1.0
1050	435.7	...			406.5	55.0	0.9	0.5
1200	193.6	5.1	214.8	0.6	269.1	2.9	13.0	0.5
LiF vapor								
77	587.6	15.1	622.5	5.7	1197.9	12.3	44.4	2.2
298	448.5	15.1	507.4	5.7	930.6	15.7	45.5	1.2
750	415.4	9.5	428.0	4.8	816.0	2.8	44.3	2.0
900	391.0	3.2	401.6	4.7	631.2	8.9	19.2	1.8
1050	416.6	27.4	435.2	32.7	461.9	16.1	1.7	0.3
1200	177.7	2.4	189.5	1.6	282.3	8.7	12.2	0.5
Vacuum								
77	516.6	8.3	526.2	9.5	1062.1	12.7	59.4	3.2
298	387.0	12.9	399.2	11.7	818.8	4.0	56.5	0.6
750	302.0	5.4	309.7	6.1	698.3	3.1	51.3	2.2
900	289.7	0.9	299.6	6.2	550.3	3.5	24.4	1.2
1050	333.1	4.8	357.6	2.7	400.3	5.3	2.3	0.3
1200	182.2	1.2	192.2	0.2	258.3	0.7	11.1	0.8

All samples were taken from their racks and weighed. A statistical summary of the relative weight changes (exposed – as-received) for the B-2 specimens exposed to the three environments at 1173 K is given in Table 2 for each period of exposure. Neither the molten-salt-exposed samples nor the LiF-vapor-exposed samples experienced any significant alteration in weight regardless of the time of exposure. In fact, most LiF exposures resulted in a very slight weight gain rather than a weight loss. The vacuum-exposed samples also gained weight during exposure, probably as a result of the nickel-base spinel and chromia films on at least part of every sample (Fig. 2a).

Metallurgical specimens to evaluate possible microstructural damage by the LiF were cut from the bread pans heat treated for 2500 and 10^4 h and compared with the as-received alloy. Clear evidence for corrosion in the molten salt regions was found inside both capsules in the form of near-surface, apparently intergranular porosity (Fig. 1b). The LiF-exposed surface of the racks (Fig. 1c) supporting the samples in the molten salt also indicated the same type and degree of attack as found in the capsule walls. While similar attack was also seen in many LiF-vapor-exposed regions, it was not uniform. Some areas had as much porosity as the liquid-LiF-exposed regions (Fig. 1b), while other areas exposed to salt vapor exhibited little sign of attack. Measurement of the depth of the porosity in the molten salt regions revealed an average depth of approximately 20 μm, with a standard deviation of about 5 μm, after either 2500 h or 10^4 h of exposure. Similar measurements in the vapor-exposed regions, where attack was found, also yielded an average depth of porosity of about 20 μm. Because the area between the Ni-shell and the B-2 capsule also contained both molten LiF and its vapor (Fig. 2b), the outer surfaces of the B-2 capsules that faced the Ni-shell were examined for signs of corrosion; however, no evidence of attack of the Hastelloy B-2 was found.

After etching, it could be seen that grain growth (Fig. 1d to f) occurred in the B-2 during exposure at 1173 K. Although there was a general tendency for the 10^4 h annealed alloy to have a larger grain size than the 2500 h heat-treated material, grain growth was not uniform. Deformation bands in the as-received sheet material (Fig. 1a) appeared to restrict grain growth in some regions; thus, bands of small grains remained in many locations after 2500 h (Fig. 1d) and 10^4 h (Fig. 1f). The eventual lateral grain growth of large grains into the bands of small grains resulted in a composite wall-like microstructure, where walls of grains were separated by grain boundaries parallel to the sheet surface (Fig. 1e). The nonuniformity of the B-2 microstructure after 1173 K annealing precluded any meaningful measurement of grain size; however, it is clear that grain growth can change the originally ~35 μm grain structure to something on the order of several hundred microns.

Examination of unetched B-2 welds revealed no signs of chemical attack by either molten LiF or its vapor in the welds themselves. After etching, the separation between the weldment and the sheet material could be readily observed (Fig. 1d), and it appears that large heat-affected zones were not formed. However, when a failed weld in B-2 was encountered, the failure was intergranular and seemed to occur at or very near the transition between recast metal and the original sheet material. Apparent intergranular-type failures were also seen in fractured rails (Fig. 1f) supporting the liquid-LiF-exposed tensile samples after either 2500 or 10^4 h of exposure.

3.1.2 Tensile Testing

Statistical summaries of the 77 to 1200 K tensile properties of as-received and exposed Hastelloy B-2 are given in Tables 3 to 6. The data reported included an arithmetic average and standard deviation (std. dev.) for each exposure condition. Blank cells in the tables are indicative of the inability to obtain any meaningful data, whereas ellipses (...) in the standard deviation cells denote conditions where triplicate testing resulted in only one or two valid tests.

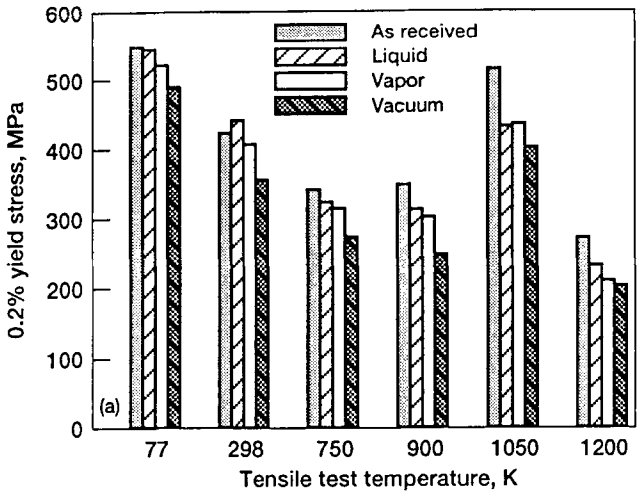

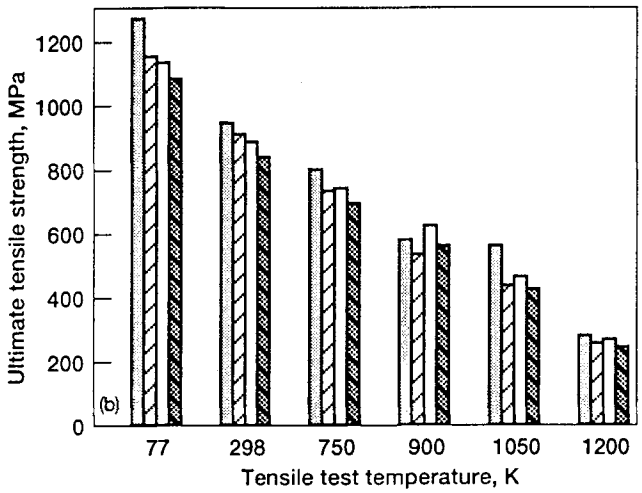

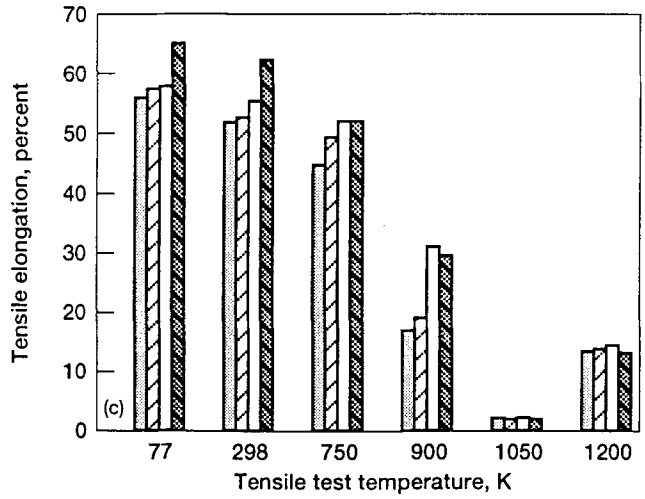

Fig. 3 Comparison of the average tensile properties of as-received Hastelloy B-2 with those after 5000 h exposure to molten LiF, its vapor, or vacuum at 1173 K. (a) 0.2% yield stress. (b) Ultimate tensile stress. (c) Tensile elongation

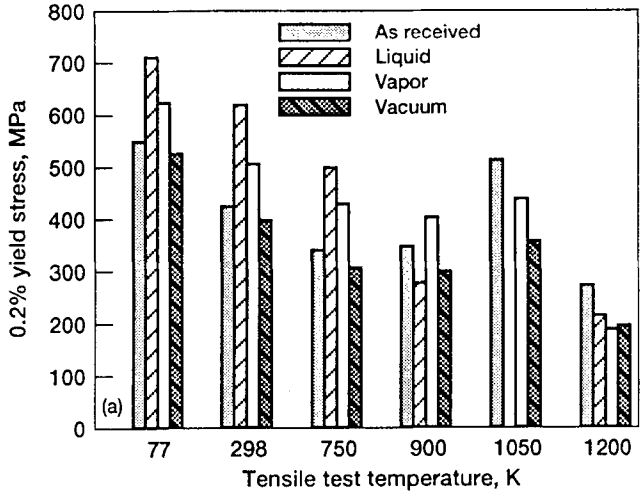

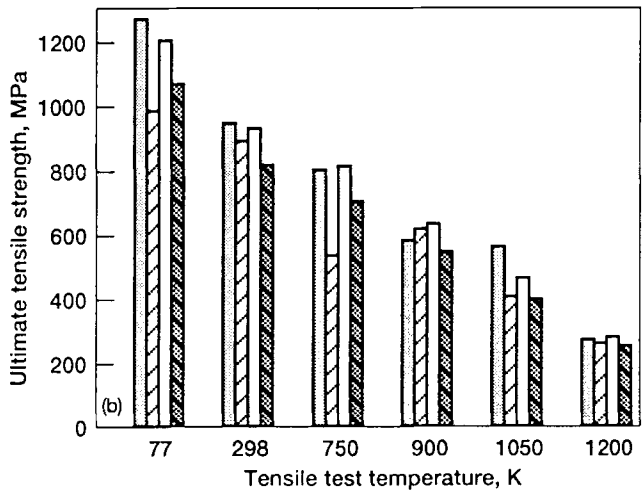

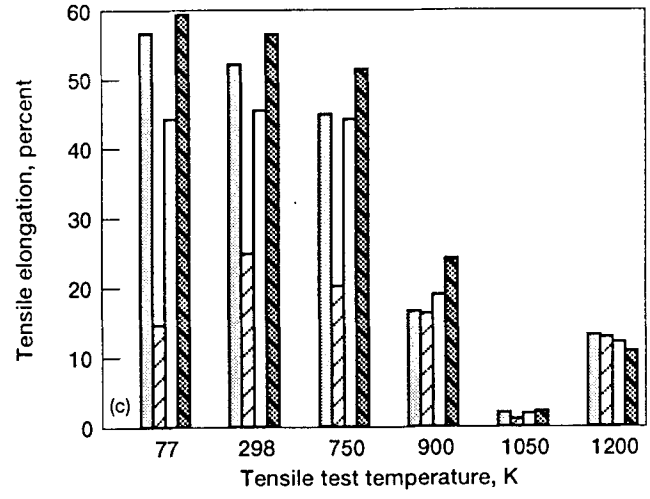

Fig. 4 Comparison of the average tensile properties of as-received Hastelloy B-2 with those after 10^4 h exposure to molten LiF, its vapor, or vacuum at 1173 K. (a) 0.2% yield stress. (b) Ultimate tensile stress. (c) Tensile elongation

Comparison of the tensile properties determined for as-received B-2 (Table 3) indicates that both testing organizations obtained similar strength and ductility values between 77 and 900 K. Because of testing difficulties, one contractor was unable to obtain valid tensile data at either 1050 or 1200 K; hence, for the purpose of further analyses, the as-received test values obtained by Cortest in Table 3 will be used to represent the initial properties of the alloy. In terms of general strength/temperature behavior, the 0.02 and 0.2% yield stress values in Table 3 indicate that strength decreases with temperature between 77 and 750 K; however, with further increases in temperature, the yield stress values initially plateau (750 to 900 K), then increase (900 to 1050 K), and finally decrease (1050 to 1200 K). The temperature dependency of the ultimate tensile strength somewhat parrots the yield stress results, except that the UTS continuously decreases with temperature through 900 K, plateaus between 900 and 1050 K, and then weakens at 1200 K. Tensile elongations are greater than 50% at and below room temperature. However, with increasing temperature the ductility decreases significantly: At 1050 K as-received B-2 displays only about 2% elongation. This trend is then reversed at 1200 K, where greater ductilities, on the order of 10%, are found.

Graphical comparisons of the tensile properties of as-received B-2 with those after 5000 and 10^4 h of exposure to LiF or vacuum at 1173 K are presented in Fig. 3 and 4, respectively. The 0.2% yield stress data in Fig. 3(a) indicate that 5000 h of exposure results in some degradation of strength, where, at any test temperature except for room temperature, the as-received material is stronger than the molten-salt-exposed material, which is, in turn, stronger than the LiF-vapor-exposed material, which is then stronger than the vacuum-heat-treated alloy. Behavior of the ultimate tensile strengths (Fig. 3b) after 5000 h of exposure generally follows the same trend exhibited by the yield strength (Fig. 3a). Concurrent with exposure leading to a general weakening, 5000 h of exposure also results in an increase in tensile elongation (Fig. 3c), except at 1050 K, where, if anything, prior exposure slightly reduces the ductility below that of as-received B-2. The most significant increase in plasticity occurs at 900 K, where prior exposure to either LiF vapor or vacuum raises the elongation to approximately 30%, compared to about 20% for the as-received condition.

Surprisingly, the relatively straightforward trends displayed after 5000 h of exposure were not observed after either 2500 h (Table 4) or 10^4 h (Fig. 4) of exposure.* In particular, the 77 to 750 K tensile elongations for B-2 after molten salt exposure are much lower than those for the as-received material. The largest degradation occurred at 77 K, where a greater than two-thirds loss of ductility (57 to ~15%) was found after molten-LiF immersions (Fig. 4c). Significant reductions, approaching a factor of two, were also seen in room-temperature and 750 K tensile elongations after contact with molten salt. While neither period of exposure had much effect on the 1200 K tensile ductility, no valid data at 1050 K were obtained after 2500 h of molten-salt immersions (Table 4), and the 10^4 h liquid-LiF-exposed samples displayed only about 1% elongation at 1050 K in contrast to the approximately 2% for as-received B-2. Lastly, there appears to be a difference in behavior between 2500 and 10^4 h molten-salt exposures on the 900 K ductility. Compared to the 900 K tensile elongation for as-received B-2, the shorter-term exposure caused embrittlement (Table 4), whereas the longer-term exposure (Fig. 4c) had essentially no effect.

In contrast to the significant effect of either 2500 or 10^4 h molten LiF on tensile elongation of Hastelloy B-2, the influence of similar-length salt-vapor exposure on ductility was much less. For example, the 77 to 750 K elongations were approximately 40% (Fig. 4c). Although this was somewhat less than the as-received values, it certainly would not be considered to be embrittlement in the manner of the 77 K ductility after molten-salt immersion. Again, a difference apparently due to length of exposure can be seen in the 900 K tensile elongations; whereas 2500 h in LiF vapor led to an almost complete loss of ductility (Table 4), the 10^4 h exposure produced 900 K elongations (Fig. 4c) greater than that for the as-received material. At the two higher tensile test temperatures (1050 and 1200 K), exposure to salt vapor seemed to produce minor reductions in ductility compared to the as-received values (Fig. 4c).

Although prior 2500 and 10^4 h exposure of Hastelloy B-2 to LiF at 1173 K had a widespread negative effect on the 77 to 1200 K tensile ductilities, similar-length vacuum exposures generally promoted increased tensile ductility compared to the as-received properties (Table 4 and Fig. 4c). But even in this case, the tensile elongation of B-2 at 1050 K was still quite low and little different from any other exposure condition. In concert with the greater tensile ductility, vacuum-exposed B-2 had lower yield stresses and ultimate tensile strengths (Fig. 4a and b) than the LiF-exposed or as-received material at essentially all temperatures.

In general, exposure to LiF changed the strength levels compared to the as-received state, where molten salt had a greater effect than the salt vapor (Fig. 4a and b). The most significant differences due to prior exposure can be seen in the higher yield strengths between 77 and 750 K (Fig. 4a), and the relatively low 77 and 750 K UTSs for molten-salt-exposed B-2 (Fig. 4b). Such low ultimate tensile strengths are probably reflections of the low 77 and 750 K tensile ductility (Fig. 4c) for this material condition.

3.1.3 Post-Tensile-Test Microstructures

Because of the large number of exposure/tensile-test temperature combinations constituting this study, only a limited number of tested Hastelloy B-2 specimens could be metallographically examined. Thus, for compatibility with 1173 K exposure of alloys 188 and 230, only the 5000 h molten-LiF, salt-vapor, and vacuum-exposed/tensile-tested B-2 samples were examined in addition to the as-received material.

No near-surface porosity was found in the as-received B-2 after tensile testing between 77 and 1200 K, as illustrated in Fig. 5(a) for a 77 K test. In the unetched state, the 77 to 750 K as-received tensile fractures appeared to be intragranular. Multiple necks were seen after 900 K testing, with part of the failure sites being intergranular. Brittle, intergranular fracture occurred at 1050 K, with numerous intergranular cracks being formed beneath the main failure site (Fig. 5b). Considerable grain-boundary cracking was also observed after 1200 K testing.

*For the sake of brevity, only examples of the behavior after 10^4 h of exposure will be noted, except where the different annealing times produced differences in mechanical properties.

The near-surface porosity found in the Hastelloy B-2 exposed to either molten LiF or its vapor (Fig. 1b) resulted in shallow surface cracks being formed during 77 to 900 K and 1200 K tensile testing (Fig. 5c). Surprisingly, similar cracks were also found in the vacuum-exposed B-2 (Fig. 5d). In any case, such surface damage did not result in premature failure, as the tensile ductility of the exposed B-2 was equal to or greater than the as-received material (Fig. 3c), and no differences in tensile fracture modes were seen. Intergranular failures were found after 1050 K tensile testing, regardless of the prior exposure condition (Fig. 5e). This behavior is similar to that in the as-received alloy, except that the smaller grain size in the as-received alloy permitted the formation of many noncatastrophic grain-boundary cracks (Fig. 5b), where this does not seem to be the case for the larger grain size B-2 after high-temperature exposure (Fig. 5e). The low ductility at 1050 K permitted an essentially undisturbed examination of long-term vacuum-exposed B-2 surfaces, and it appears that a second phase formed in the surface-connected grain boundaries (Fig. 5f). Energy-dispersive analysis of the second phase in a scanning electron microscope indicated that this phase was highly enriched with aluminum (~20 wt%), compared to a low matrix level (<0.4 wt%). The source of this impurity is not known.

3.2 *Haynes Alloy 188*

3.2.1 Exposure

Following the planned 1173 K vacuum heat treatment of the Ni-shell-encased alloy 188 bread pan, the LiF/vacuum-ex-

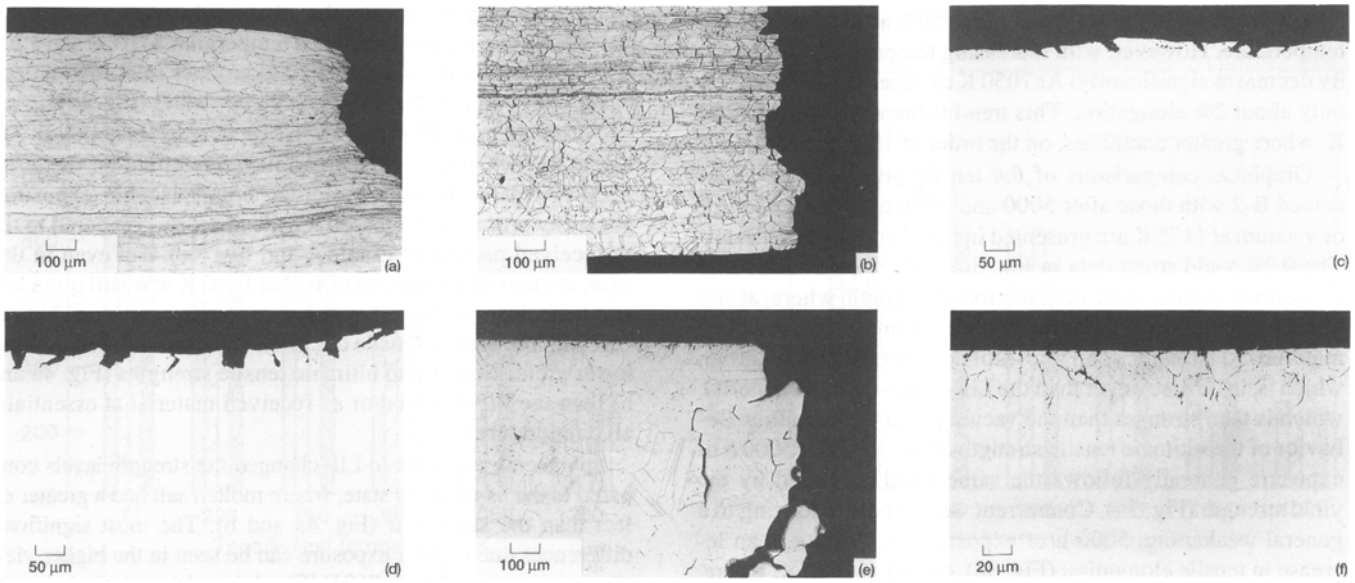

Fig. 5 Typical microstructures in tensile tested as-received and 5000 h, 1173 K exposed Hastelloy B-2. (a) As-received alloy tested at 77 K. (b) As-received alloy tested at 1050 K. (c) Molten-LiF-exposed alloy tested at 77 K. (d) Vacuum-exposed alloy tested at room temperature. (e) Molten-LiF-exposed alloy tested at 1050 K. (f) Vacuum-exposed alloy tested at 1050 K. (a, b, e) Etched. (c, d, f) Unetched

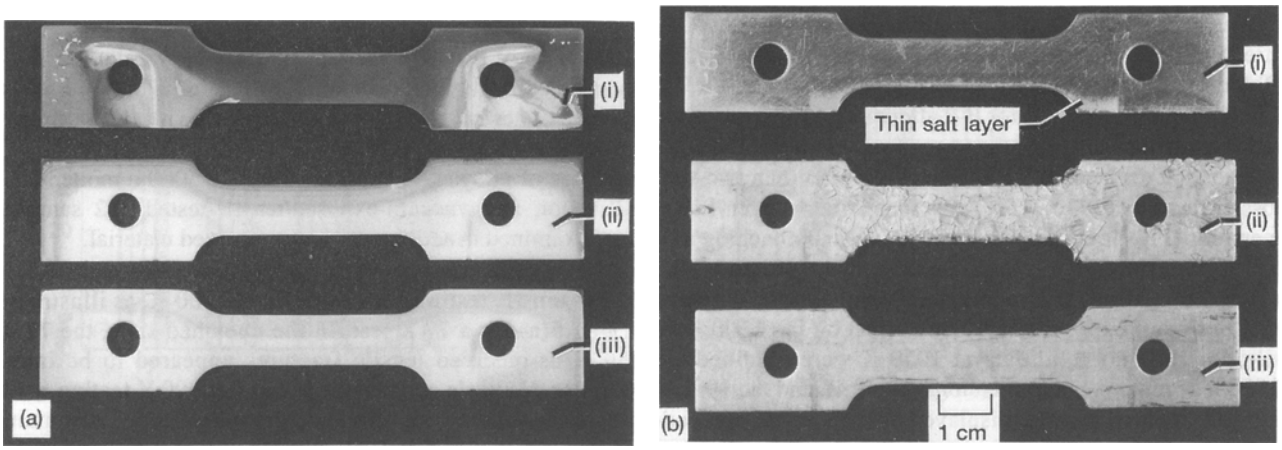

Fig. 6 Photographs of vacuum- and LiF-exposed Haynes alloy 188 after 5001.3 h at 1173 K. (a) Vacuum-exposed specimen (i) with a heavy coating, (ii) with a typical coating, and (iii) after being wiped. (b) LiF-exposed samples: (i) salt vapor, (ii) molten salt, and (iii) molten salt after scraping and a 1 h 1173 K vacuum anneal

posed tensile samples were examined and weighed. The vacuum-exposed alloy 188 samples were covered in regions of dark and light gray matte finishes: Areas facing away from the top of the capsule (toward the furnace heat shields) were dark gray, whereas areas pointing toward the top of the capsule were lighter gray. Figure 6(a) presents photographs of vacuum-heat-treated alloy 188 samples illustrating examples of the most extensive coating and a typical coating. Part of the coating on the vacuum-exposed samples was powdery and tended to fall off during handling. Chemical analysis of the loose powder indicated that it was mainly tungsten. The vacuum-exposed alloy 188 samples were weighed without wiping and after wiping with a clean rag (Table 7).

After the Ni-201 shell and side wall of the alloy 188 bread pan had been cut through, the inside of this capsule appeared much the same as that shown in Fig. 2(b), except that the rack of LiF-vapor-exposed tensile samples was not bent. The salt-vapor-exposed samples were a dull metallic color. In addition, they had salt on edges facing toward the molten salt bath and thin salt coatings partially covering each sample. A photograph of a typical LiF-vapor-exposed alloy 188 sample illustrating the extent of the thin salt coating on the gage section is presented in Fig. 6(b). Prior to weighing the vapor-exposed samples, the thicker salt deposits on the specimen edges were scraped away.

The frozen block of LiF encasing the molten-salt-exposed samples was bonded to the inside walls of the alloy 188 bread pan and required significant effort to free it. Once removed, visual examination of the block of salt revealed that it had a yellowish layer directly beneath the rack of tensile specimens, while transparent LiF existed everywhere else. Chemical analysis, however, of a number of samples taken from various regions in the frozen LiF failed to reveal any impurities. Because the frozen salt tenaciously bonded to most of the alloy 188 specimens, protracted mechanical manipulation was required to separate them. Even then, large amounts of LiF remained firmly attached to specimens (Fig. 6b); hence, it was necessary to scrape the samples with a metal tool to remove the majority of the LiF. Despite this procedure, it was obvious that thin coatings of salt still covered large areas on each sample; therefore, the specimens were subjected to a 1 h vacuum heat treatment at 1173 K to drive off the remaining LiF. As shown in Fig. 6(b), this procedure seemed to be effective in removing the remaining salt.

Statistical summaries of the relative weight change results for alloy 188 after being exposed to vacuum or LiF for 5001.3 h at 1173 K are given in Table 7. For completeness, the changes for molten-salt-exposed samples after being just scraped and scraped + 1 h in vacuum at 1173 K as well as the data for wiped and unwiped vacuum-exposed specimens are presented. Clearly, the second cleaning step for either the molten-salt or vacuum-exposed samples made a difference in the results and thus gave a more accurate estimate of potential attack. Based on the weight loss experienced by the alloy 188 specimens immersed in the molten LiF, it appears that some minor attack did occur. The existing data for the salt-vapor-exposed material indicate a slight weight gain (Table 7). However, because of (1) the presence of LiF on these samples (Fig. 6b) and (2) the effect of a 1 h/1173 K vacuum heat treatment on the molten-salt-exposed specimens, it is likely that the LiF-vapor-exposed alloy 188 samples also experienced a small weight loss rather than a gain. Lastly, wiping away the loose tungsten-rich coating on the vacuum-heat-treated samples only increased the magnitude of the weight loss experienced by these specimens, which on average lost about 2 mg/cm^2.

Metallurgical samples were taken from the alloy 188 capsule to assess possible damage by LiF.* Only slight roughening on LiF-exposed surfaces (Fig. 7), possibly in combination with narrow alloy depletion zones, was found. Measurement of the grain size away from the LiF-exposed surfaces gave an average value of 29 μm, with a standard deviation of 4.7 μm. This represents an approximate 50% increase in grain diameter compared to the as-received alloy.

*A description of the microstructures found on the exterior surface of the alloy 188 bread pan that was encased in the Ni-shell is given in the Appendix.

Table 7 Statistical summary of the relative weight changes of Haynes alloy 188 and alloy 230 after exposure to various environments at 1173 K

	(Exposed – as received)(a), mg/cm^2				
	Molten salt		Salt vapor	Vacuum	
Material	Scraped	1 h at 1173 K in vacuum		Not wiped	Wiped
Alloy 188 (5001.3 h)					
Average	0.22	–0.21	0.34	–1.19	–1.71
Std. dev.	0.11	0.03	0.14	0.48	0.19
Maximum	0.48	–0.14	0.82	2.02(b)	–1.29
Minimum	0.04	–0.27	0.08	–1.61	–2.14
Alloy 230 (5000 h)					
Average	0.20	–0.14	3.81	–0.96	–0.98
Std. dev.	0.10	0.13	0.60	0.17	0.15
Maximum	0.46	–0.02	5.43	0.18	–0.49
Minimum	0.02	–0.62	1.94	–1.55	–1.64

(a) Data from about 50 specimens for each condition, where each sample has about 33 cm^2 of surface area and weighs about 16 g. (b) First sample in rack of specimens; the only specimen that gained weight.

3.2.2 Room-Temperature Tensile Testing

Triplicate tensile tests on as-received and LiF/vacuum-exposed Haynes alloy 188 were conducted. Typical stress-strain curves from each of four exposure conditions are presented in Fig. 8(a), and a statistical summary of the room-temperature tensile properties is given in Table 8. The stress-strain diagrams indicate little difference in behavior for the three salt/vacuum environmental conditions through 7% strain. However, the prolonged exposure to 1173 K did initially soften alloy 188 with respect to the as-received condition, and this weakening is reflected in the lower 0.2% yield strength values (Table 8). Beyond approximately 3% strain, the exposed alloys were stronger than the as-received material (Fig. 8a), but the ultimate tensile strengths of all four material conditions were similar (Table 8). In terms of tensile elongation, there appeared to be some degradation due to 1173 K exposure, where the ~62% for as-received material dropped to about 50% for molten-salt-exposed material and then to approximately 42% for the LiF-vapor and vacuum-exposed material. Metallurgical examination of selected unetched room-temperature tensile specimens, however, revealed no evidence of corrosive attack in either the molten-LiF, salt-vapor, or vacuum-exposed conditions. In particular, the unetched gage sections of the tested samples were free of any signs of surface disruptions as found in the vacuum-exposed B-2 samples (Fig. 5d and f). After etching, a thin carbide-free surface layer was seen in the sample exposed to vacuum (Fig. 7c), which correlates with a loss of volatile elements (Table 7).

3.3 *Haynes Alloy 230*

3.3.1 Exposure

This bread-pan capsule, which had not been encased in a Ni-shell, was vacuum heat treated for 5000 h at 1173 K. Both the outside of the capsule and the vacuum-exposed samples were covered with regions of dark and light gray matte finishes. The appearance of the vacuum-exposed alloy 230 specimens was the same as that of the alloy 188 samples (Fig. 6a): Areas facing away from the top of the capsule were dark gray, whereas areas pointing toward the top of the capsule were lighter gray. While the coating on the vacuum exposed samples was powder-like, it was much more tenacious than that found on alloy 188. However, for consistency, the alloy 230 specimens were first weighed, with care being taken to preserve the coating, and then they were wiped and reweighed. As was the case for the vacuum-exposed alloy 188 samples, analysis of the coating on vacuum-exposed alloy 230 also indicated that it was mainly tungsten.

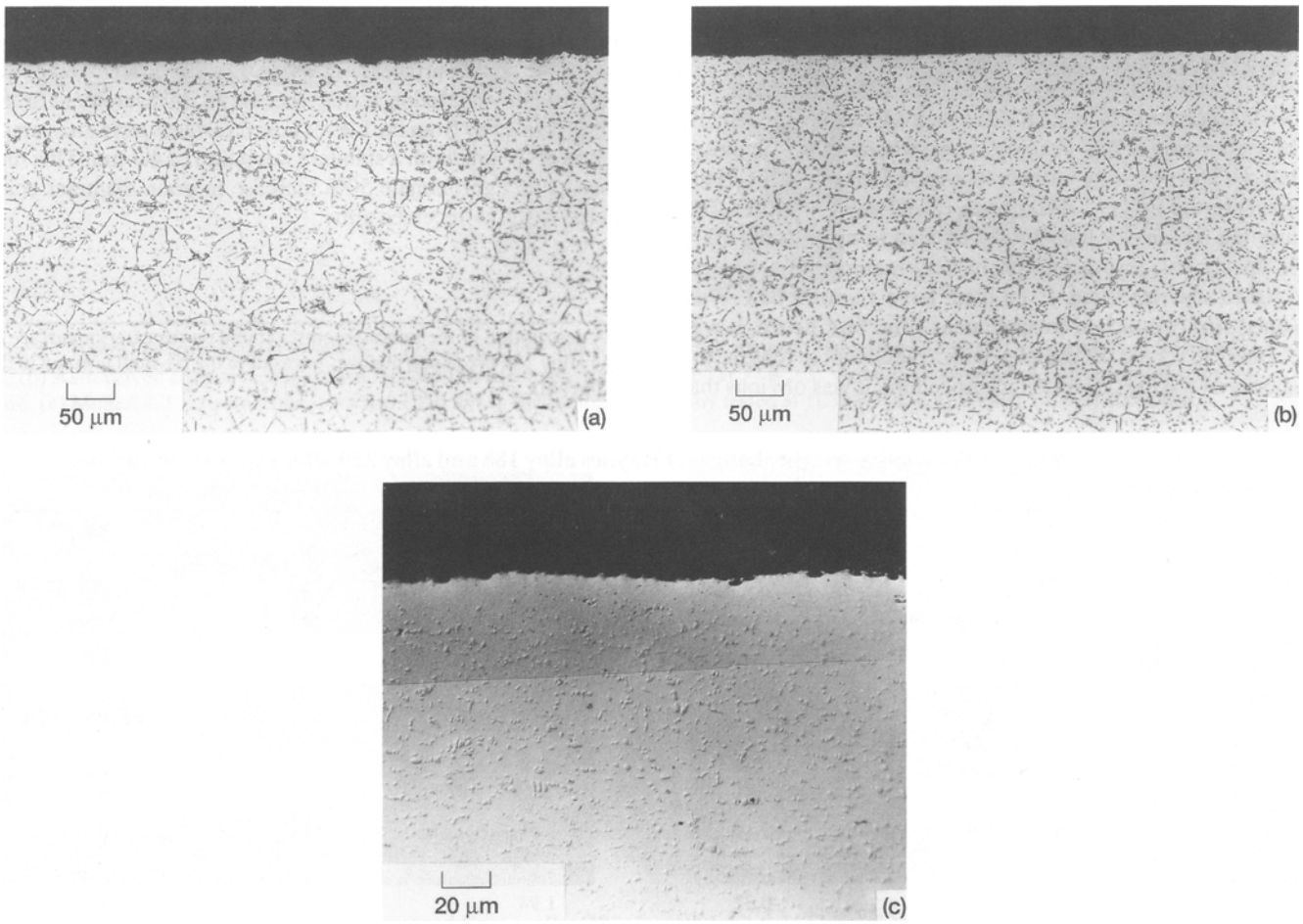

Fig. 7 Typical microstructures in Haynes alloy 188 after 5001.3 h exposure at 1173 K. (a) Molten LiF. (b) LiF vapor. (c) Gage section of a room-temperature tensile-test specimen after being exposed to vacuum

Opening of the capsule revealed geometry identical to that shown in Fig. 2(b), except that the rack of salt-vapor-exposed samples was not bent. The internal side wall of the bread pan had a dull gray metallic color in both the molten-LiF and salt-vapor-exposed regions. The LiF-vapor-exposed tensile samples also had a dull matte gray color, with darker shading in areas facing away from the molten salt. Considerable salt was splashed on the vapor-exposed samples in large and small drops as well as in thin sheen coatings. Because of the extensive coverage, no attempt was made to remove this salt before weighing the vapor-exposed specimens.

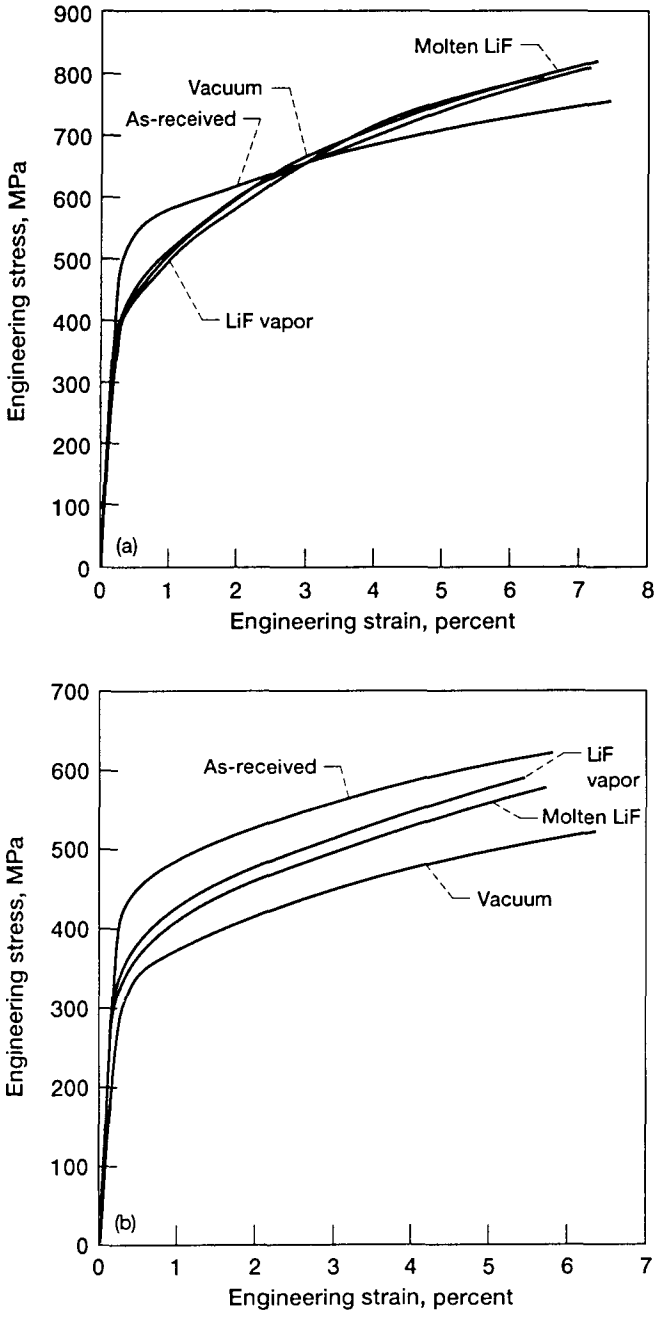

Fig. 8 Engineering stress-strain diagrams for as-received and ~5000 h LiF/vacuum-exposed specimens. (a) Haynes alloy 188. (b) Haynes alloy 230.

The main block of frozen salt had transparent regions and areas of white color. Chemical analysis of frozen salt samples taken from various regions revealed no impurities. After the tensile samples were broken out of the frozen LiF, they possessed a dull matte gray metallic finish, and most alloy 230 specimens had salt bonded to them in the same manner as the alloy 188 samples (Fig. 6b). While each alloy 230 sample was carefully scraped clean, not all the LiF could be removed. Hence, they were also given a 1 h vacuum heat treatment at 1173 K to drive off the remaining salt.

Statistical summaries of the relative weight change data for LiF/vacuum-exposed alloy 230 samples are presented in Table 7. The results for the molten-salt-exposed specimens indicated that some attack occurred, which produced, on average, a small loss. All the vapor-exposed specimens experienced relatively large weight gains (~4 mg/cm^2), which is probably reflective of the extensive salt splashes on the samples rather than a corrosion product. As opposed to the behavior of vacuum-exposed alloy 188 samples, the tungsten coating on alloy 230 was much more firmly bonded and could not be removed by simple wiping. Despite this behavior, the data reveal that vacuum exposure of alloy 230 at 1173 K will result in the loss of mass.

Microstructural examination of samples cut from the 1173 K heat-treated alloy 230 capsule revealed extensive near-surface damage in the material directly exposed to vacuum (Fig. 9a and b). Defects such as isolated pores and agglomerated porosity (cracks) are clearly visible in unetched samples (Fig. 9a). Furthermore, the decreasing ability to etch grain boundaries and the lack of second phases in an approximately 450 μm wide band, as the vacuum-exposed-surface is approached (Fig. 9b), indicates a probable loss of chromium through volatilization. The extent of porosity/cracking was less in weldments exposed to vacuum than that found in the base sheet alloy. In general, unetched samples revealed that prolonged exposure of alloy 230 to either molten LiF or its vapor produced only a roughened surface; however, two isolated regions of relatively severe intergranular attack and intragranular porosity (Fig. 9c) were noted in LiF-vapor-exposed alloy 230. After etching of the LiF-exposed alloy 230, an approximately 50 μm second phase-free surface layer was visible (Fig. 9d); again, the absence of definite grain boundaries in this region compared to the underlying alloy is indicative of the loss of alloying elements. Measurement of the grain size on etched samples gave an average value of 32 μm, with a standard deviation of 3.7 μm, which is essentially identical to the as-received grain dimensions.

3.3.2 Room-Temperature Tensile Testing

A summary of results from triplicate room-temperature tensile testing of as-received and LiF/vacuum-exposed alloy 230 is given in Table 8, and typical stress-strain curves are shown in Fig. 8(b). These plots indicate that all the 1173 K exposure conditions weaken the alloy with respect to the as-received state through at least 7% strain. Both Fig. 7(b) and the average tensile strength properties (Table 8) point out that prior vacuum exposure produced the largest loss in strength, while exposure to either molten LiF or its vapor generated an intermediate strength degradation. The salt atmospheres, however, led to an approximate 20% relative loss in ductility compared to the as-

Table 8 Room-temperature tensile properties of Haynes alloy 188 and alloy 230 after exposure at 1173 K

Exposure condition	0.2% Yield stress, MPa		UTS, MPa		Elongation, %	
	Average	Std. dev.	Average	Std. dev.	Average	Std. dev.
Alloy 188 (5001.3 h)						
As received	540.6	6.4	1037.8	1.1	61.9	2.2
Molten LiF	441.2	10.8	1044.8	0.7	49.0	0.0
LiF vapor	436.9	6.9	1043.6	5.8	42.5	1.3
Vacuum	415.8	16.1	984.8	25.4	41.4	0.4
Alloy 230 (5000 h)						
As received	448.3	5.2	891.7	3.4	55.0	1.5
Molten LiF	357.1	6.4	830.2	8.8	42.4	2.3
LiF vapor	370.4	3.7	849.8	3.1	45.5	1.6
Vacuum	335.9	0.5	810.9	6.3	63.1	0.8

received condition, while vacuum exposure increased the average elongation about 15%.

Examination of the unetched microstructure of the failed room-temperature tensile alloy 230 specimens revealed no examples of severe attack or premature failure. After etching, both the molten-salt-exposed and vacuum-exposed tensile-tested specimens had carbide-free surface regions, but the depth of these regions was about 50 μm after LiF exposure (Fig. 9e) and perhaps twice that after vacuum exposure (Fig. 9f).

4. Discussion

A considerable amount of data involving microstructural observations after long-term 1173 K exposure to LiF or vacuum and post exposure tensile properties has been generated for three different wrought superalloys in this study. From these results it can be concluded, as outlined below, that Hastelloy B-2 is probably not a suitable alloy for containment of LiF. Furthermore, based on the minor corrosion of B-2 by LiF, it appears that impurities in the salt will not result in indefinite, self-sustaining chemical reactions that could destroy any superalloy. As the degree of this corrosion is governed by the loss of hydrogen, it can be generally shown that impurity-induced attack will be limited in all alloys that are permeable to hydrogen. Likewise, it can be reasoned that the solubility of the metal fluorides will restrict the extent of reaction between any thermal energy storage vessel containing a limited amount of salt. Lastly, the use of Cr(Mn)-containing superalloys at high temperatures in a vacuum is considered, and the results for Haynes alloys 188 and 230 reconfirm a safe, unrestricted upper-use temperature limit of about 1100 K.

The most telling observation with regard to Hastelloy B-2/LiF bread-pan capsules was the fracturing of the racks holding the tensile specimens in the molten LiF (Fig. 2c). This finding, in conjunction with the low 1050 K tensile ductility measured in the as-received alloy or B-2 specimens after 1173 K exposures (Fig. 3 and 4), confirms that embrittlement of Hastelloy B-2 at high temperatures will occur when this alloy is used as a containment alloy for molten LiF. Failure of the specimen racks probably occurred during heat-up, when thermal expansion (or volume change on melting) of the salt exerted sufficient stress to cause the rack to fracture. Hence, the fractures in the racks (Fig. 1f) are similar in appearance to those after 1050 K tensile testing (Fig. 5e). Although the B-2 bread-pan capsules themselves were not affected by the volume change of the LiF or the high-temperature brittleness, it is clear that B-2 parts encased within the salt can be injured. Secondly, the bending of the B-2 rack supporting the LiF vapor-exposed tensile samples (Fig. 2a) indicates that this alloy might not possess sufficient strength to maintain its shape at temperature. In view of these results, Hastelloy B-2 does not appear to be the appropriate choice for containment of LiF or any other thermal energy storage salts that melt at temperatures on the order of 1100 K.

The essentially equal depths of attack in Hastelloy B-2 exposed to molten LiF for either 2500 or 10^4 h at 1173 K (Fig. 1b and c) indicate that this corrosion was probably related to impurities in the salt rather than to a basic incompatibility between LiF and the alloy. Furthermore, the release of hydrogen from B-2 capsules in Ni-shells (which poisoned the cryogenic pumps) suggests that chemical attack from impurities within a LiF thermal energy storage vessel might be self-limiting. For example, water entrained in the salt should react with the capsule wall (Ref 2) via:

$$2LiF + H_2O = Li_2O + 2HF \quad \text{(Eq 1)}$$

$$xMe + yHF = Me_xF_2 + y/2H_2 \quad \text{(Eq 2)}$$

where Me represents cobalt, chromium, iron, nickel, and so on. If hydrogen permeates through the container wall, reactions (1) and (2) will then be driven to completion. The amounts (partial pressures) of H_2O, HF, and H_2 will approach zero, and corrosion via these equations will cease. Such behavior should be quite general regardless of the containment alloy composition. The only necessity is that hydrogen be able to permeate through the alloy and be lost to some sink (for example, the vacuum of space). With the loss of hydrogen, a self-sustaining corrosion mechanism originating from water in LiF is simply not possible.

Interactions between LiF and the chromium-containing superalloys Haynes alloy 188 (Fig. 7a and b) and alloy 230 (Fig. 9d and e) were also seen. At least for alloy 230, there appears to be a much greater attack than one would expect from simple impurities in the salt alone. This might be due in part to the relatively high solubility of CrF_2 in LiF at 1173 K (Ref 2), which would result in near-surface chromium depletion zones, that is,

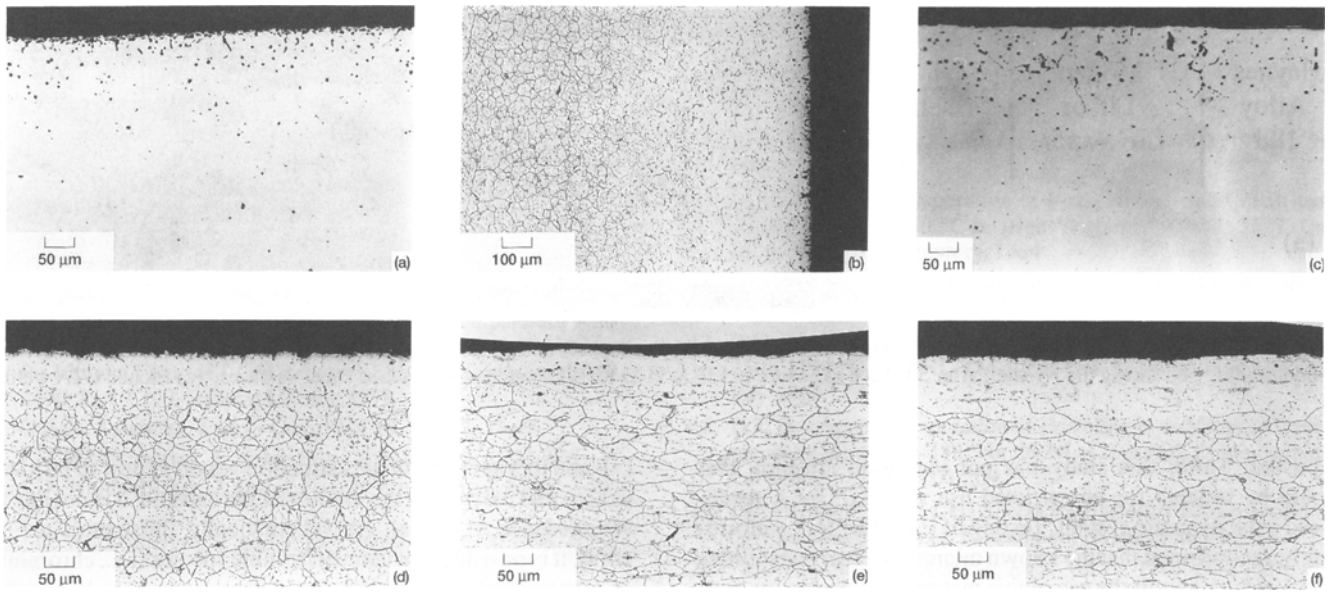

Fig. 9 Typical microstructures in vacuum- and LiF-exposed Haynes alloy 230 after 5000 h at 1173 K. (a) (b) Vacuum-exposed surfaces. (c) Area of high attack in LiF vapor. (d) Molten-LiF-exposed surface. (e) Gage section of a room-temperature tensile-test specimen after being exposed to LiF vapor. (f) Gage section of a room-temperature tensile-test specimen after being exposed to vacuum. (a, c) Unetched. (b, d-f) Etched

carbide-free surface layers (Fig. 9d and e). Corrosion via this mechanism, however, should be limited in scope, because (1) the salt in a thermal energy storage vessel is a closed system, and (2) the reaction will stop once the solubility limit for CrF_2 in LiF is reached.

While attack between LiF and the chromium-containing superalloys due to impurities in the salt or the solubility of CrF_2 in LiF should be limited in scope, the loss of volatile elements to the vacuum of space would not be restricted. In this study, the infinite sink capacity of space was simulated by vacuum exposure when volatilized elements were directly lost to the furnace heat shields, other Cr(Mn)-deficient metals acting as sinks, or cold sections of the furnace. For cases where these conditions were met (i.e., the sides and bottom of the bread-pan capsule), significant microstructural damage occurred (Fig. 9a and b) in the form of ~35 μm deep surface cracks, a ~100 μm wide band containing Kirkendall pores, and a ~450 μm carbide depletion zone. Such a carbide-free band represents about 35% of the sheet thickness used in this study. Clearly, this degree of microstructural damage should have some measurable effect on postexposure mechanical properties. However, as can be seen in Fig. 8(b) and Table 8, there is little difference in the room-temperature properties between LiF and vacuum-exposed alloy 230. The apparent negligible losses following vacuum exposure are probably due to the geometry of the experiment, where tensile samples arranged side by side in racks could be simply transferring Cr(Mn) back and forth to each other and losing relatively little to the vacuum. Such behavior has been well documented for 1093 K vacuum exposure of both alloys 188 and 230 (Ref 13); unfortunately, similar effects cannot be directly shown in this study at 1173 K due to the deposition of tungsten on the tensile samples.

In summary, the probable effect(s) of 1173 K vacuum exposure on Cr(Mn)-containing superalloys depends on the local environment. If other chromium-rich alloys are located in the near vicinity and are in the line of sight, then the loss of volatile elements will tend to be small and the damage to the microstructure minimized. However, if no other sources of Cr(Mn) are located nearby and/or they are out of the line of sight, then essentially all volatilized material will be lost and significant microstructural damage will take place. Obviously, over a sufficient time at temperature, this latter behavior will seriously affect the mechanical properties of the alloy. Based on the efforts of Bourgette (Ref 15-18), 1100 K has been generally recognized as the upper temperature limit for the unrestricted use of chromium-containing metals in vacuum. Comparison of studies of alloys 188 and 230 at 1173 K and at 1093 K (Ref 13) tends to reconfirm that 1100 K is a valid boundary. Specifically, for alloy 188 a vacuum exposure for 22,500 h at 1093 K (Ref 13) did not produce a large weight change in unshielded samples (estimated 1.6 mg/cm^2), whereas 5000 h at 1173 K in the current work produced a weight loss of 1.7 mg/cm^2 in shielded samples (Table 2). Thus, comparison of the worst case at 1093 K against the best case at 1173 K indicates that the acceptable maximum-use temperature in vacuum must be around 1100 K.

Lastly, three other points should be noted. First, comparison of the average residual tensile ductilities of Hastelloy B-2 following either 5000 h (Fig. 3) and 2500 h (Table 4) or 10^4 h (Fig. 4) exposures to molten LiF at 1173 K reveals a paradox. Whereas the short- and long-term exposures indicate significant losses in low-temperature elongations, the intermediate period revealed enhanced ductilities. The cause for this divergent behavior is not known. Second, the low-temperature tensile embrittlement similar to that experienced by both Haynes alloys 188 and 230 after 1093 K exposures (Ref 9-14) was not found after 1173 K heat treatments of those two alloys. The 80 K increase in temperature resulted in minimum room-temperature elongations of 40% compared to 10 to 20% after 1093 K

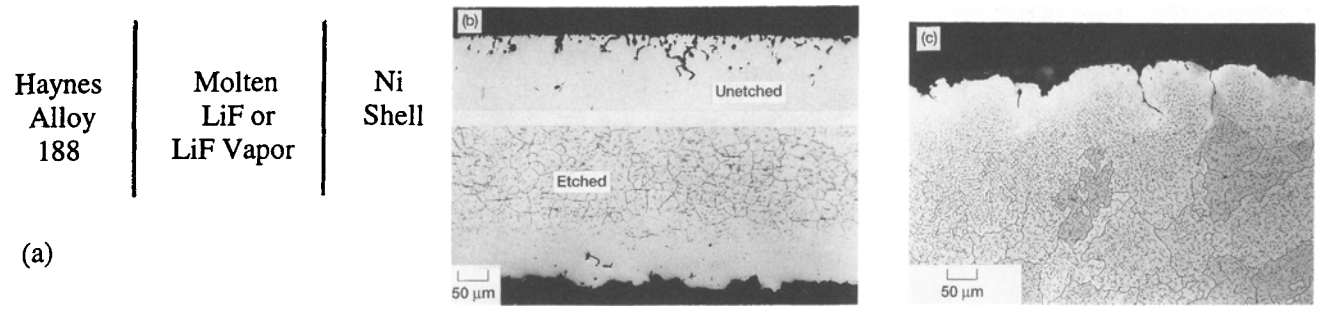

Fig. 10 Schematic of the geometry between Haynes alloy 188 bread-pan capsule and Ni-shell (a) and typical microstructures in the Haynes alloy 188 facing the Ni-shell after 5001.3 h exposure to LiF at 1173 K: (b) Unetched and etched sheet surfaces, (c) Etched GTA weld

exposure. Third, this study has not identified an alloy that would be suitable for unrestricted use with LiF for a space-based solar dynamic system. Testing of Hastelloy B-2, unfortunately, reconfirmed that the known microstructural instabilities (Ref 19) would limit the use of this material. Furthermore, testing of more traditional chromium-containing superalloys indicated that open vacuum exposures will lead to alloy (second-phase) depletion zones. Although chromium-bearing alloys could be suitable for vacuum environments where volatile element loss can be minimized, a totally acceptable containment alloy for LiF remains to be identified.

5. Summary of Results

In attempt to determine the suitability of several superalloys for the long-term containment of molten LiF, Hastelloy B-2, Haynes alloy 188, and Haynes alloy 230 have been exposed to LiF and vacuum at 1173 K. While not significantly affected by either the salt or vacuum, low strength at elevated temperatures and microstructural instabilities leading to negligible ductility at 1050 K appear to preclude the use of the low-volatile-element-content Hastelloy B-2 for this application. Other than relatively narrow chromium (second-phase) depletion zones, the chromium-containing Haynes alloys 188 and 230 were not significantly attacked by LiF; however, unrestricted vacuum exposures produced wide depletion bands: approximately 450 μm after 5000 h. Such damage seems to limit the usefulness of volatile-element-containing superalloys for storage of LiF in vacuum.

Acknowledgments

The author would like to acknowledge the Advanced Solar Dynamics group at the NASA Lewis Research Center for funding of the experiment effort. In addition, he would like to recognize Prof. Eduard Arzt for the opportunity to spend a year at Max-Planck-Institut für Metallforschung; the Alexander von Humboldt foundation for partial financial support while at Max-Planck-Institut für Metallforschung; and the NASA-Lewis Research Center for granting the leave of absence.

Appendix

Being encased in a Ni-201 shell, the exterior surface of the alloy 188 bread-pan capsule was directly exposed to molten LiF and its vapor. While this situation would appear to be identical to that existing in the interior of the capsule, it is not due to the presence of nickel. As schematically illustrated in Fig. 10(a), it is possible that volatile/soluble species (i.e., chromium or manganese) in alloy 188 could be permanently lost to the nickel either by vapor or liquid transport through the LiF-containing region. This seems to be the case, as a surprising amount of near-surface microstructural damage was found on the alloy 188 walls and welds facing the Ni-shell. Figure 10(b) illustrates unetched and etched alloy 188 sheet that has experienced severe damage in the form of pores and cracks, and Fig. 10(c) shows the microstructure of a GTA weld after etching. The porosity, lack of etching, and apparent decrease in size and number of second phases near the surface in Fig. 10(b and c) are indicative of loss of alloying elements.

Although the exterior of the alloy 188 capsule was not directly exposed to vacuum, where the vacuum itself acts as a sink for volatile elements, the Ni-shell appears to behave as a sink since it has a high solubility for chromium. In essence, the geometry illustrated in Fig. 10(a) approximates the exposure of alloy 188 to a "pure" vacuum environment. Thus, it can be concluded that Haynes alloy 188 exposed to vacuum at 1173 K will undergo the same type of damage as experienced by Haynes alloy 230 (Fig. 9a and b). This contention is confirmed by the carbide-free layer in vacuum-exposed, tensile-tested alloy 188 samples (Fig. 7c).

Lastly, it should be pointed out that the Hastelloy B-2 bread pans were also encapsulated in Ni-201 and heat treated at 1173 K, yet no apparent microstructural damage was visible (Fig. 1 d and e). The most obvious reasons for this behavior would be (1) the low content of volatile alloying elements (Table 1) and (2) the lack of solubility of molybdenum in LiF and/or the non-volatility of molybdenum. All these factors would prevent the loss of alloying constituents from B-2 to the Ni-shell.

References

1. T.L. Labus, R.R. Secunde, and R.G. Lovely, "Solar Dynamic Power for Space Station Freedom," NASA TM-102016, National Aeronautics and Space Administration, 1989
2. A.K. Misra and J.D. Whittenberger, Fluoride Salts and Container Materials for Thermal Energy Storage Applications in the Temperature Range 973-1400 K, *Energy—New Frontiers* (IECEC '87), American Institute of Astronautics and Aeronautics, 1987, p 188-201
3. J.D. Whittenberger and A.K. Misra, *J. Mater. Eng.*, Vol 9, 1987, p 293-302

4. H.J. Strumpf and M.G. Coombs, Solar Receiver for the Space Station Brayton Engine, *Proc. Gas Turbine Conference and Exhibition,* ASME Paper 87-GT-252, American Society of Mechanical Engineers, 1987
5. R.C. Schulze, "The Corrosion of Superalloys by Lithium Fluoride in a Cyclic High Temperature Corrosion Environment," NASA CR-54781, National Aeronautics and Space Administration, 1965
6. J.N. Mattavi, F.E. Heffner, and A.A. Miklos, "The Sterling Engine for Underwater Vehicle Applications," Paper 690731, Society of Automotive Engineers, 1969, p 2376-2400
7. E.R. Cprek, "Metallurgical Studies of High Temperature Alloy Capsules after Long Time Cyclic Corrosion Tests as Containers for Lithium Fluoride," GM Research Laboratories Report GMR-2690, Part 7.109, General Motors, 1978
8. G.A.A. Asselman, *Energy Conv.,* Vol 16, 1976, p 35-47
9. J.D. Whittenberger, *J. Mater. Eng.,* Vol 12, 1990, p 211-226
10. J.D. Whittenberger, *J. Mater. Eng. Perform.,* Vol 1, 1992, p 469-482
11. J.D. Whittenberger, *J. Mater. Eng. Perform.,* Vol 3, 1994, p 754-762
12. J.D. Whittenberger, T *J. Mater. Eng. Perform.,* Vol 3, 1994, p 763-774
13. J.D. Whittenberger, *J. Mater. Eng. Perform.,* Vol 2, 1993, p 745-757
14. J.D. Whittenberger, *J. Mater. Eng. Perform.,* Vol 3, 1994, p 91-103
15. D.T. Bourgette, "Evaporation of Iron-, Nickel- and Cobalt-base Alloys at 760 to 980 °C in High Vacuums," ORNL-3677, Oak Ridge National Laboratory, 1964
16. D.T. Bourgette and H.E. McCoy, *Trans. ASM,* Vol 59, 1966, p 324-339
17. D.T. Bourgette, "Vaporization Phenomena of Haynes Alloy No. 25 to 1150 °C," ORNL-TM-1786, Oak Ridge National Laboratory, 1967
18. D.T. Bourgette, "Evaporation of Hastelloy N and Haynes Developmental Alloy No. 188," in ORNL-4250, Oak Ridge National Laboratory, 1970, p 204-209
19. Haynes International Data Sheets for Hastelloy B-2 and personal communication with M. F. Rothman, Haynes International
20. J.D. Whittenberger, *J. Mater. Eng.,* Vol 10, 1988, p 247-258